IEICE TRANS. COMMUN., VOL.E94–B, NO.3 MARCH 2011

PAPER

Bending-Loss Insensitive Fiber with Hole-Assisted Structure

Kazuhide NAKAJIMA[†a)], **Tomoya SHIMIZU**[†], **Takashi MATSUI**[†], **Chisato FUKAI**[†], *and* **Toshio KURASHIMA**[†], *Members*

SUMMARY The characteristics of hole-assisted fiber (HAF) are investigated both numerically and experimentally in terms of its applicability as a bending-loss insensitive fiber (BIF). We show that HAF with the desired mode-field diameter (MFD), bending-loss and cutoff wavelength characteristics can be roughly designed by taking a few specific structural parameters into consideration. We also show that an optical cord composed of adequately designed HAF realizes satisfactory transmission performance with respect to its multi-path interference (MPI) characteristics. These results reveal that a hole-assisted type BIF will be beneficial for realizing easy and economical installation and maintenance in future access networks.

key words: *hole-assisted fiber, bending-loss, mode field diameter, cutoff wavelength, multi-path interference*

1. Introduction

Recently, fiber to the home (FTTH) has been deployed widely because of the growing demand for broadband services. A bending-loss insensitive fiber (BIF) is expected to be a key medium since it will be useful for realizing the easy and economical installation and maintenance of FTTH networks. Moreover, BIF for use in access networks has already been standardized as ITU-T Recommendation G.657, and the latest version supports a minimum bending radius of 5 mm [1]. With this as the background, various BIFs have been intensively researched and developed [2]–[5].

Hole-assisted fiber (HAF) is an attractive light guide that can be realized simply by adding several air holes around a conventional doped core. This hole-assisted structure provides various unique characteristics [6]. Recent reports also indicate the applicability of HAF as a high power light guide [7], [8]. We can consider HAF as a candidate for BIF, whose ultimately low bending-loss characteristics are particularly attractive [9], [10]. However, the strong confinement effect of air holes also affects the higher order mode. This makes it very important to clarify in detail the transmission characteristics of fiber with a hole-assisted structure.

In this paper, we discuss the characteristics of HAF in relation to its use as a BIF. In Sect. 2, we investigate the optimum design of a hole-assisted type BIF both numerically and experimentally. Here, we clarify that the mode-field diameter (MFD), bending-loss and cutoff wavelength characteristics of HAF can be roughly designed taking a few specific structural parameters into consideration [11]. In Sect. 3, we discuss the transmission characteristics of HAFs with different cross-sectional parameters experimentally. The multi-path interference (MPI) characteristics of HAF based optical cords are also investigated in this section. As a result, we show that properly designed HAF can be used as BIF in future access networks.

Manuscript received August 24, 2010.
Manuscript revised November 12, 2010.

[†]The authors are with NTT Access Network Service Systems Laboratories, NTT Corporation, Tsukuba-shi, 305-0805 Japan.
a) E-mail: nakaji@ansl.ntt.co.jp

DOI: 10.1587/transcom.E94.B.718

2. Design Considerations

Figure 1 shows a cross-sectional image of the HAF that we discuss in this paper. We assumed a conventional germanium doped step index type core with diameter 2a and relative index difference Δ. Here, the cladding was composed of pure silica glass. N air holes with diameter d were arranged around the core. In Fig. 1, $N = 10$ is shown as an example. The inscribed and circumscribed radii are described as R_{In} and R_{Out}, respectively.

In this paper, we defined the air filling fraction S as the ratio of air holes in the region surrounded by inscribed and circumscribed circles [11]. Thus, S can be described as Eq. (1).

$$S \equiv \frac{N(d/2)^2}{R_{Out}^2 - R_{In}^2} \tag{1}$$

We then examined the structural parameter dependence of the MFD, bending-loss and cutoff wavelength in HAF.

2.1 MFD Characteristic

It is well known that the MFD in a conventional step index

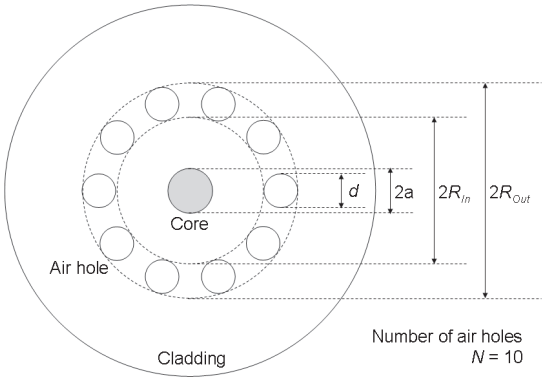

Fig. 1 Cross sectional image of HAF.

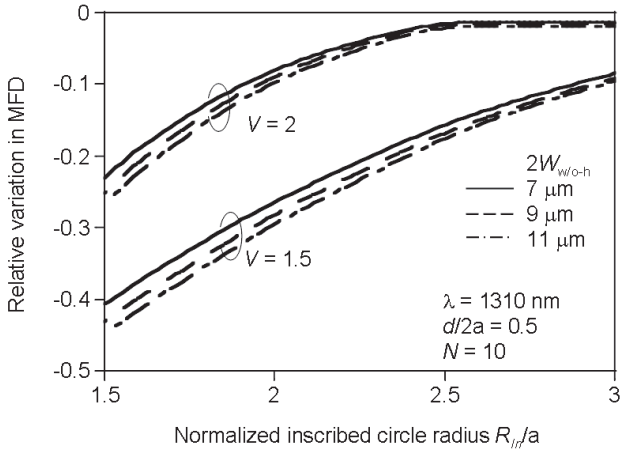

Fig. 2 Relative variation in MFD as a function of normalized inscribed circle radius R_{In}/a calculated at 1310 nm.

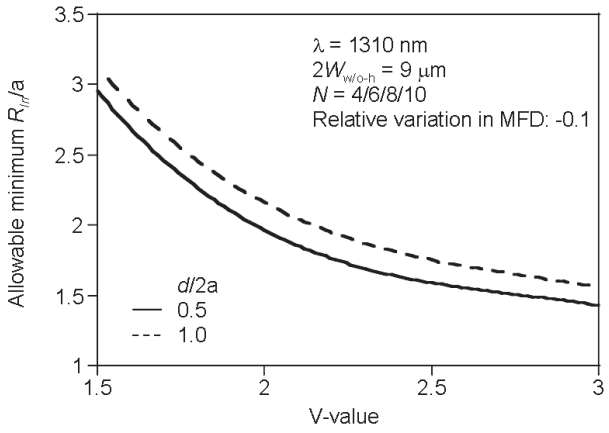

Fig. 3 Allowable minimum R_{In}/a as a function of V value when the relative variation in MFD was set at −0.1 at 1310 nm.

fiber can be derived using Eq. (2) [12].

$$W \approx a \times \left(0.65 + 1.619\, V^{-1.5} + 2.879\, V^{-6}\right) \tag{2}$$

Here, W represents the mode-field radius. V denotes the V parameter, which is determined using the 2a and Δ values. The MFD characteristics of HAF are also closely related to the R_{In} value. In this study, we examine the relationship between the V parameter and R_{In} in a hole-assisted structure.

Figure 2 shows the relative variation in MFD as a function of the normalized inscribed circle radius R_{In}/a calculated at 1310 nm. The normalized air hole diameter d/2a and N were set at 0.5 and 10, respectively. We also defined the MFD with and without air holes as $2W$ and $2W_{w/o-h}$, respectively. The relative variation in the MFD was assumed to be $\equiv (2W_{w/o-h} - 2W)/2W_{w/o-h}$. The solid, dashed and dash-dotted lines show the results when we assumed $2W_{w/o-h}$ values of 7, 9 and 11 μm, respectively. Two set of curves represent different V parameters of 1.5 and 2. It should be noted that the V parameters were directly calculated using the 2a and Δ values of the core by simply neglecting the air holes. Figure 2 confirms that the MFD in HAF decreases greatly as the R_{In}/a value decreases. Smaller MFD increases the splice loss at a certain lateral offset [12]. Excessive variation in MFD degrades the splice loss particularly when the air holes are vanished by arc fusion. Figure 2 also reveals that the relative variation in MFD is more sensitive to the V value than $2W_{w/o-h}$. We then derive the minimum R_{In}/a value by assuming the allowable relative variation in MFD.

Figure 3 shows the calculated minimum R_{In}/a characteristic as a function of the V parameter. The relative variation in the MFD was set at −0.1, and $2W_{w/o-h}$ was 9 μm at 1310 nm. A 9 μm MFD is a typical value of a conventional 1.3 μm zero-dispersion wavelength single-mode fiber (SMF) [13]. A 0.1 relative variation also corresponds to the MFD tolerance in the conventional SMF, and this enables to reduce the MFD mismatch induced splice loss to less than 0.05 dB [12]. The solid and dashed lines show the results when the d/2a values were 0.5 and 1.0, respectively. Both results show the average allowable minimum R_{In}/a when we assumed N = 4, 6, 8 and 10 air holes. Figure 3 shows that we can derive the minimum R_{In}/a value using the V parameter of the core although there is a slight dependence on d/2a. These results reveal that the MFD in HAF can be roughly controlled by knowing the allowable minimum R_{In}/a value, which is determined using the V parameter of the core and the desired relative variation in the MFD. For example, the following approximate function can be considered.

$$(R_{In}/a)_{\min} \approx m_1 + m_2 V + m_3 V^2 + m_4 V^3 \tag{3}$$

Here, m_i (i = 1, 2, 3 and 4) denotes the coefficient, and we obtained $m_1 \approx 12.8$, $m_2 \approx -11.2$, $m_3 \approx 3.9$ and $m_4 \approx -0.5$ when we employed the dashed line in Fig. 3.

2.2 Bending-Loss and Cutoff Wavelength Characteristics

The bending-loss α_b and cutoff wavelength λ_c characteristics of HAF were investigated with regard to S and Δ dependence. Figures 4(a) and (b) show the S dependence of α_b and λ_c, respectively. α_b was evaluated at 1625 nm and a bending radius r of 5 mm. The filled circle shows the result obtained with a conventional SMF. The open symbols show the results obtained with HAFs with different S values. The R_{In}/a values were in the 1.2 to 3.5 range. The open circles and squares show the HAFs where N = 6 and 10, respectively. It should be noted that all the samples including the SMF had similar 2a and Δ values of 9 μm and 0.35%, respectively. λ_c of all samples were measured by using the transmitted power technique with multimode reference [14]. The solid line shows the calculated results when we assumed a HAF where R_{In}/a = 2.0 and N = 10. We defined the λ_c of HAF as the wavelength at which the confinement loss of the first higher order mode reaches 1 dB/m [15].

Figure 4 confirms that the measured and calculated results reveal a similar tendency. It is also found from Fig. 4(a) that the α_b of the HAF improves exponentially as the S value increases. As for the λ_c characteristics, Fig. 4(b) confirms that λ_c tends to be longer in proportion to the S value, and it is particularly strongly affected when S exceeds 0.45. This

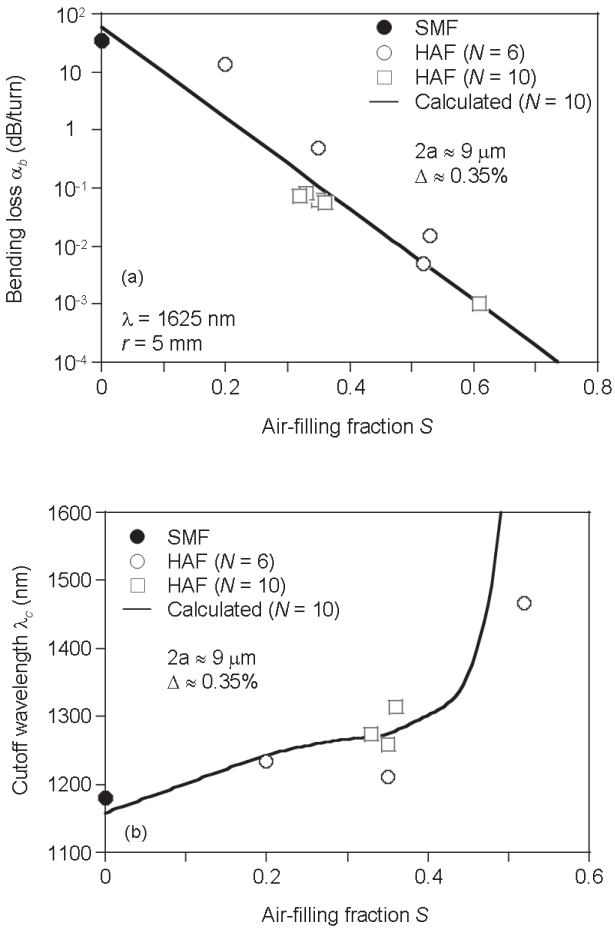

Fig. 4 Air filling fraction S dependences of (a) bending loss α_b and (b) cutoff wavelength λ_c.

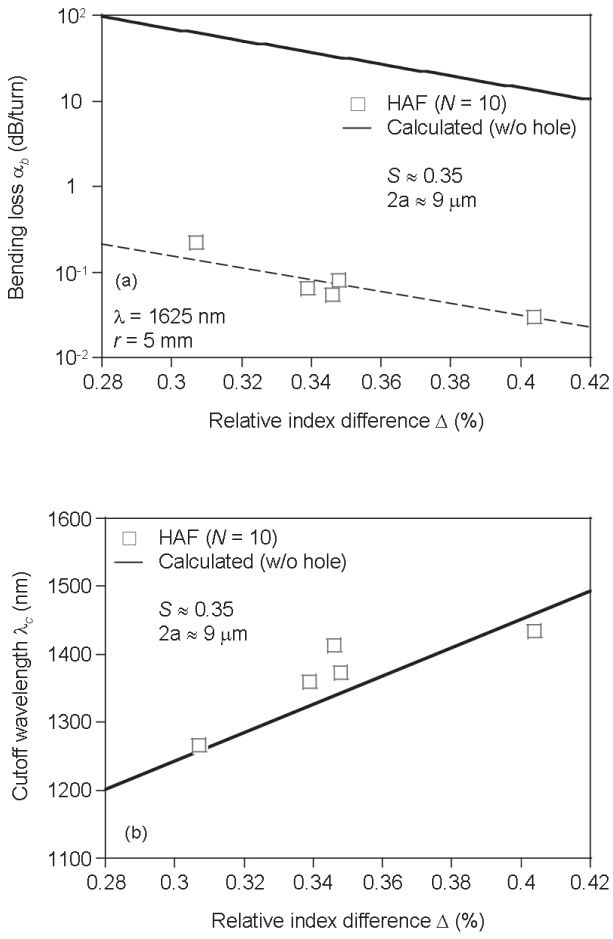

Fig. 5 Relative index difference Δ dependences of (a) bending-loss α_b and (b) cutoff wavelength λ_c.

is because the region surrounded with air holes supports another guided mode. The confinement loss of the corresponding mode to be less than 1 dB/m at 1550 nm when S exceeds 0.45. Moreover, the effective index of this mode becomes larger than that of the 1st higher order mode in the wavelength region of 1600 nm or longer. This results in the rapid change in λ_c at a larger S value.

Figures 5(a) and (b) show the Δ dependence of α_b and λ_c, respectively. The open squares show the results obtained with HAFs with different Δ values. In this case, all the HAFs with $N = 10$ had similar 2a and S values of 9 μm and 0.35, respectively. The solid line shows the calculated results when we assumed a conventional SMF without air holes. The dashed line in Fig. 5(a) is shown for comparison, and it is completely parallel to the solid line. Thus, Figs. 5(a) and (b) confirm that the Δ dependence of α_b and λ_c in HAF can be considered similar to that in a conventional SMF.

Strictly speaking, the α_b and λ_c characteristics of HAF are also related to the individual R_{In}/a, d/2a and N values. However, these results show that the α_b or λ_c characteristic of HAF can be roughly estimated taking into account the exponential or linear dependence on the S and Δ values. As a result, we can derive two empirical relations as follows.

$$\ln(\alpha_b) \approx \ln(b_1) + b_2 \cdot S + b_3 \cdot \delta\Delta \quad (4)$$

$$\lambda_c \approx c_1 + c_2 \cdot S + c_3 \cdot \delta\Delta \quad (5)$$

Here, b_i and c_i (i = 1, 2 and 3) show the coefficients, and $\delta\Delta$ is defined as the difference in relation to an arbitrary reference value. In this study, we can empirically derive the b_2 value of our HAF as -18 by applying the least mean square method to the results shown in Fig. 4(a). As for c_2, we can also obtain 337 (for $S \leq 0.45$) or 8543 (for $S > 0.45$) using Fig. 4(b).

2.3 HAF with Desired Characteristics

Taking the previous discussion into account, we can easily derive the optimum design conditions for HAF with desired characteristics. For example, we assumed the following requirements for our HAF. $2W_{w/o-h}$ and λ_c values were determined by taking into account the typical characteristics of a conventional SMF [13].

i) $2W_{w/o-h}$ must be 9 μm or more and the relative variation in the MFD should be more than -0.1 at 1310 nm,
ii) α_b should be less than 0.5 dB/turn at 1625 nm and r = 5 mm,

iii) λ_c should be 1260 nm or shorter.

Figure 6 shows the calculated relationship between the S and Δ values when we set 2a at 8 μm. The solid line shows the α_b condition obtained with Eq. (4), and we can expect an α_b of less than 0.5 dB/turn at 1625 nm and at r = 5 mm in the region to the right of the solid line. The dashed line shows the λ_c requirement derived with Eq. (5), and a λ_c of shorter than 1260 nm can be obtained to the left of the dashed line. Therefore, we can design HAF with the desired α_b and λ_c characteristics by setting the S and Δ values in the region surrounded by the solid and dashed lines. In Fig. 6, we can also derive the corresponding V and Δ values as 2.3 and 0.35%, respectively, if we substitute the 2a of 8 μm and the $2W_{w/o-h}$ requirement of 9 μm into Eq. (2). We then directly determined the minimum and maximum S values as 0.26 and 0.40, respectively. Thus, we can obtain the optimum design conditions by considering the arbitrary core diameter.

Figure 7 shows the optimum design conditions for HAF that satisfies the $2W_{w/o-h}$, α_b and λ_c requirements. The left and right figures show the 2a conditions as a function of the S and Δ values, respectively. Figure 7 reveals that HAF with the desired characteristics can be expected by designing the S, 2a and Δ values in the 0.25–0.53, 6.0–8.2 μm and 0.323–0.370% ranges, respectively. As an example, we designed the 2a and Δ values at 7.8 μm and 0.34%, respectively. The corresponding V value becomes 2.24. Then, the

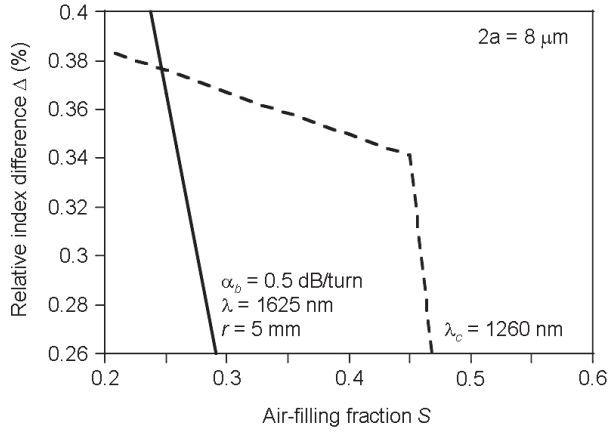

Fig. 6 Calculated relationship between air filling fraction S and relative index difference Δ when we set 2a at 8 μm.

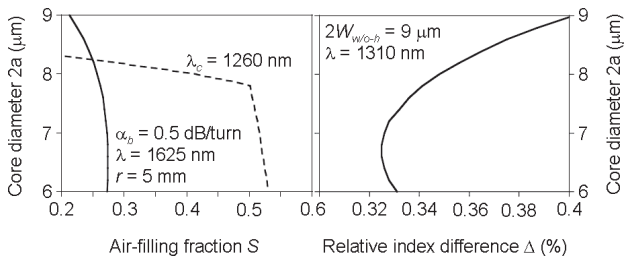

Fig. 7 Optimum design conditions for HAF with desired MFD, bending-loss and cutoff wavelength characteristics.

allowable minimum R_{In}/a can also be derived as 1.7 by using Eq. (3). Thus, HAF with the desired characteristics can be obtained by controlling the inscribed circle radius and the air hole diameter so that the R_{In}/a and S values are more than 1.7 and in the 0.26–0.50 range, respectively. As a result, we clarified that HAF with the desired MFD, bending-loss and cutoff wavelength can be roughly designed using the specific structural parameters of V, S and Δ.

3. Experiments and Discussion

3.1 Properties of HAF

We then fabricated HAFs with different structural parameters taking the previous discussion into consideration. Table 1 summarizes the characteristics of three HAFs. HAF1 and 2 had similar 2a and Δ values of 7.8 μm and 0.31%, respectively. The 2a and Δ values of HAF3 were set at slightly larger values than the other HAFs. The N values of HAF1 and 2 were 6 and 10, respectively. The (S, R_{In}/a) values of HAF1 and 2 were designed to be (0.49, 2.1) and (0.41, 2.8), respectively, so that the requirements i) to iii) described in Sect. 2.3 were satisfied simultaneously. By contrast, the S value of HAF3 with 6 air holes was set at 0.60 for comparison, but R_{In}/a was designed to be 2.0 to maintain the relative variation in MFD at more than −0.1. Table 1 confirms that HAF1 and 2 meet the MFD, α_b and λ_c requirements. It is also seen that with HAF3 an extremely low α_b of less than 0.01 dB/turn was achieved with a satisfactory mode-field characteristic, although λ_c becomes longer than 1600 nm. These results well support the expected properties as described in the previous section.

It is also noted from Table 1 that the zero-dispersion slope S_0 of the fabricated HAFs tends to be large compared with that of conventional SMF. Moreover, a slight shortening in the zero-dispersion wavelength λ_0 can be seen in HAF3. Figure 8 shows the calculated λ_0 (left side axis) and S_0 (right side axis) as a function of R_{In}/a. The 2a, Δ, S and N values were set at 9.0 μm, 0.3%, 0.4 and 10, respectively, as examples. Two dashed lines with an arrow indicate the λ_0 and S_0 values without the air holes. Figure 8 confirms that λ_0 becomes shorter as R_{In}/a decreases. Moreover, a 30%

Table 1 Characteristics of fabricated HAFs.

		HAF1	HAF2	HAF3
Core diameter 2a	(μm)	7.8	7.8	9.0
Relative index difference Δ	(%)	0.31	0.31	0.36
Air-filling fraction S		0.49	0.41	0.60
Normalized inscribed circle radius R_{In}/a		2.1	2.8	2.0
Number of air holes N		6	10	6
Bending-loss α_b (@1625 nm, r = 5 mm)	(dB/turn)	0.05	0.04	<0.01
Cutoff wavelength λ_c	(nm)	1118	1126	>1600
MFD $2W$ (@1310 nm)	(μm)	8.9	9.0	8.7
Zero-dispersion wavelength λ_0	(nm)	1318	1321	1290
Zero-dispersion slope S_0	(ps/nm^2·km)	0.098	0.090	0.102

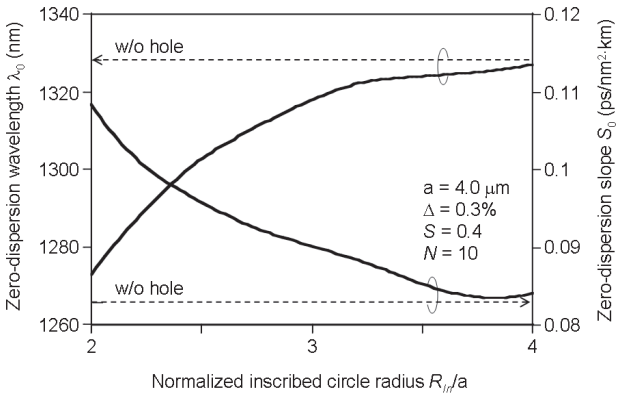

Fig. 8 Calculated zero-dispersion wavelength λ_0 and zero-dispersion slope S_0 as a function of normalized inscribed circle radius R_{In}/a.

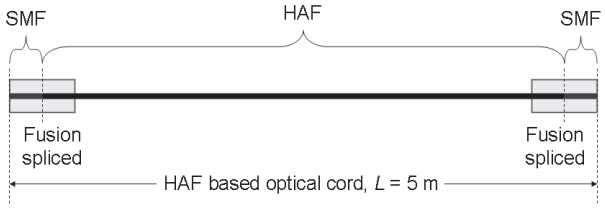

Fig. 9 Schematic image of HAF based optical cord.

Table 2 Insertion and return losses of HAF based optical cords.

			Cord1 (with HAF1)	Cord2 (with HAF2)	Cord3 (with HAF3)
Insertion loss	(dB)	Ave.	0.15	0.11	0.21
		Max.	0.25	0.22	0.29
		Min.	0.08	<0.01	0.14
Return loss	(dB)	Ave.	51.8	51.2	54.3
		Max.	52.2	52.1	55.3
		Min.	51.2	49.0	52.8

λ = 1550 nm

Sample number: 10

enlargement in the S_0 can be found when R_{In}/a is reduced to 2.0. These results reveal that the chromatic dispersion characteristics of HAF are also sensitive to the R_{In}/a value.

3.2 Applicability of HAF

A relatively short HAF based optical cord will be an attractive application when we consider HAF as a candidate for BIF. The endface of HAF should generally be appropriately sealed to prevent any air hole contamination. We therefore prepared a 5 m long optical cord using HAF1–3. Figure 9 shows a schematic image of the fabricated HAF cord. A conventional SMF was fusion spliced to both ends of the HAF to protect the air holes. A conventional SC connector was attached, and the other end of the SMF was adequately polished.

Table 2 summarizes the insertion and return losses of the HAF based optical cords measured at 1550 nm. In this

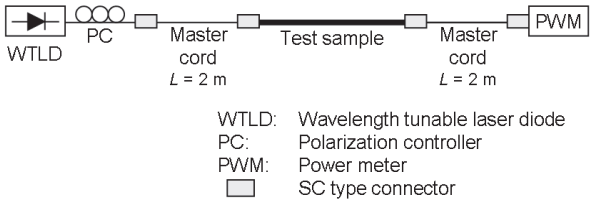

Fig. 10 Experimental setup for measuring MPI.

experiment, we used a conventional SMF with an MFD of 8.6 μm at 1310 nm and a cutoff wavelength of less than 1260 nm. There were 10 samples. Table 2 confirms that satisfactory low insertion losses were achieved independent of the HAF characteristics since the MFD values of all the HAFs were comparable to that of the SMF. We also found that all the HAF based optical cords had good return loss characteristics. These results show that endface termination with fusion spliced SMF is beneficial for realizing a HAF based bending-loss insensitive optical cord.

Superior light confinement achieved using the hole-assisted structure also affects the higher order mode. Moreover, HAF3 has a longer cutoff wavelength characteristic. It can be considered that the modal noise in HAF may degrade the transmission characteristics. We then examined the multi-path interference (MPI) characteristics [16], [17] of our HAF. Figure 10 shows the experimental setup we used for measuring the MPI [17]. We used an external cavity type wavelength tunable laser diode (WTLD) as a light source. The cw light from the WTLD was guided into a test sample via a polarization controller (PC) and a 2 m long master cord, which consisted of conventional SMF. The light transmitted through another master cord was detected with an optical power meter (PWM). Then, the MPI of the test sample was evaluated using the peak-to-peak value of the received power.

Figure 11 shows the MPI characteristics of the HAF based optical cords. The upper and lower parts of the figure show the results measured at 1310 and 1550 nm, respectively. The filled circles and bars show the average and maximum/minimum levels for 10 samples. Here, the reference MPI was evaluated by replacing HAF based optical cord with 5 m long SMF cord. Figure 11 confirms that the MPI of the HAF based optical cords was comparable to the reference level independent of wavelength and type of HAF. Moreover, it should be noted that we can expect negligible influence on both analog and digital transmission performance if we ensure an MPI of less than −50 dB [18].

Figure 12 shows the relative degradation in MPI as a function of the bending radius r. The measurement wavelength was 1550 nm and the number of bends was set at 10. The filled circles show the results obtained with the conventional SMF. The open circles, triangles and diamonds show the results obtained with HAF1, 2 and 3, respectively. Figure 12 shows that the MPI in the SMF was degraded as the r value decreased. This is because the leaked light induced by a small bend interferes with the guided light. Reference [18]

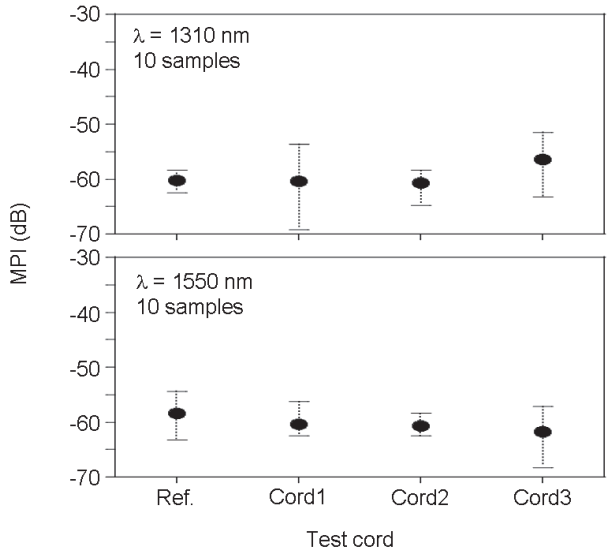

Fig. 11 MPI of HAF based optical cord measured at 1310 nm (upper) and at 1550 nm (lower).

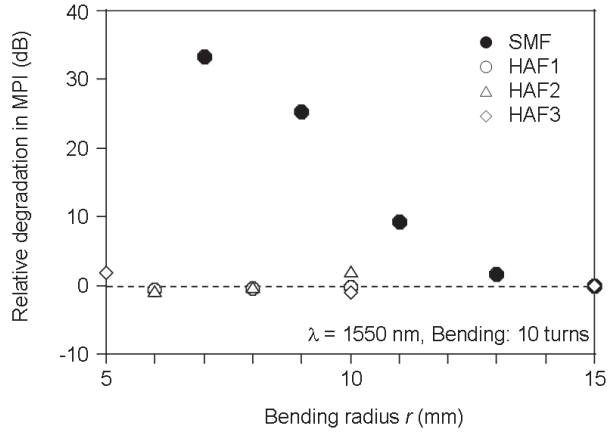

Fig. 12 Relative variation in MPI as a function of bending radius r.

also reported that a bending-loss of more than 1 dB clearly degrades the MPI characteristic. By contrast, no noticeable MPI degradation was observed for any of the HAFs even under bending conditions consisting of a 5 mm radius and 10 turns. As a result, we found that a bending-loss insensitive HAF with an adequate termination is beneficial for realizing flexible optical wiring. Moreover, HAF with the optimum structural design is a candidate for reliable single-mode BIF that can be used in future FTTH networks.

4. Conclusions

We investigated the characteristics of HAF as a BIF candidate both numerically and experimentally. We clarified that HAF with the desired MFD, bending-loss and cutoff wavelength characteristics can be roughly designed using the specific structural parameters represented by the V, S and Δ values. We also confirmed that HAF based optical cord with an appropriate termination can be used as a solution for flexible optical wiring in terms of MPI characteristics. These results showed that a hole-assisted type BIF will be beneficial for realizing easy and economical installation and maintenance in future access networks.

Acknowledgments

We thank M. Tsubokawa and Y. Sakuyama for their continuous encouragement.

References

[1] ITU-T, Recommendation G.657, Characteristics of a bending-loss insensitive single-mode optical fibre and cable for the access network, 2nd ed., Nov. 2009.
[2] K. Himeno, S. Matsuo, N. Guan, and A. Wada, "Low-bending-loss single-mode fibers for fiber-to-the-home," J. Lightwave Technol., vol.23, no.11, pp.3494–3499, 2005.
[3] M.J. Li, P. Tandon, D.C. Bookbinder, S.R. Bickham, M.A. McDermott, R.B. Desorcie, D.A. Nolan, J.J. Johnson, K.A. Lewis, and J.J. Englebert, "Ultra-low bending loss single-mode fiber for FTTH," Proc. OFC'08, PDP10, 2008.
[4] J.M. Fini, P.I. Borel, M.F. Yan, S. Ramachandran, A.D. Yablon, P.W. Wisk, D. Trevor, D.J. DiGiovanni, J. Bjerregaard, P. Kristensen, K. Carlson, P.A. Weimann, C.J. Martin, and A. McCurdy, "Solid ring-assisted fibers with low bend loss," Proc. OECC'08, ThN2, 2008.
[5] L.-A. de Montmorillon, F. Gooijer, N. Montaigne, S. Geerings, D. Boivin, L. Provost, and P. Sillard, "All-solid G.652.D fiber with ultra low bend losses down to 5 mm bend radius," Proc. OFC'09, OTuL3, 2009.
[6] T. Hasegawa, E. Sasaoka, M. Onishi, M. Nishimura, Y. Tsuji, and M. Koshiba, "Novel hole-assisted lightguide fiber exhibiting anomalous dispersion and low loss below 1 dB/km," Proc. OFC'01, PD5, 2001.
[7] K. Takenaga, S. Tanigawa, S. Matsuo, M. Fujimaki, and H. Tsuchiya, "Fiber fuse phenomenon in hole-assisted fibers," Proc. ECOC'08, P.1.14, 2008.
[8] N. Hanzawa, K. Kurokawa, K. Tsujikawa, T. Matsui, and S. Tomita, "Suppression of fiber fuse propagation in photonic crystal fiber (PCF) and hole assisted fiber (HAF)," Proc. MOC'09, M7, 2009.
[9] J. Zhou, K. Nakajima, K. Tajima, K. Hogari, K. Sato, and I. Sankawa, "Application of hole-assisted type PCF with good bending loss performance," Proc. IWCS2003, pp.48–52, 2003.
[10] K. Nakajima, K. Hogari, J. Zhou, K. Tajima, and I. Sankawa, "Hole-assisted fiber design for small bending and splice losses," IEEE Photonics Technol. Lett., vol.15, no.12, pp.1737–1739, 2003.
[11] K. Nakajima, T. Shimizu, C. Fukai, T. Kurashima, and M. Shimizu, "Single-mode hole-assisted fiber with low bending loss characteristics," Proc. IWCS'09, 9-3, 2009.
[12] D. Marcuse, "Loss analysis of single-mode fiber splice," Bell Syst. Tech. J., vol.56, no.5, pp.703–718, 1977.
[13] ITU-T, Recommendation G.652, "Characteristics of a single-mode optical fibre cable," 8th ed., Nov. 2009.
[14] ITU-T, Recommendation G.650.1, "Definitions and test methods for linear, deterministic attributes of single-mode fibre and cable," 6th ed., July 2010.
[15] T. Matsui, K. Nakajima, and C. Fukai, "Applicability of photonic crystal fiber with uniform air-hole structure to high-speed and wide-band transmission over conventional telecommunication bands," J. Lightwave Technol., vol.27, no.23, pp.5410–5416, 2009.
[16] C.X. Yu, W. Wang, and S.D. Brorson, "System degradation due to multipath coherent crosstalk in WDM network nodes," J. Lightwave Technol., vol.16, no.8, pp.1380–1386, 1998.
[17] S. Ramachandran, J.W. Nicholson, S. Ghalmi, and M.F. Yan, "Measurement of multipath interference in the coherent crosstalk regime," IEEE Photonics Technol. Lett., vol.15, no.8, pp.1171–1173, 2003.

[18] C. Fukai, K. Nakajima, T. Shimizu, T. Matsui, Y. Goto, and T. Kurashima, "Relationship between optical wiring conditions and MPI degradation," Proc. OFC'10, OWA1, 2010.

Kazuhide Nakajima received M.E. and Ph.D. degrees in electrical engineering from Nihon University, Chiba, Japan, in 1994 and 2005, respectively. In 1994, he joined NTT Access Network Systems Laboratories, Tokai, Ibaraki, Japan, where he engaged in research on optical fiber design and related measurement techniques. He is currently a Senior Research Engineer of NTT Access Network Service Systems Laboratories, Tsukuba, Ibaraki, Japan.

Tomoya Shimizu received B.E. and M.E. degrees in electronic engineering from Tohoku University, Sendai, Japan, in 2000 and 2002, respectively. In 2002, he joined NTT Access Network Service Systems Laboratories, Tsukuba, Ibaraki, Japan, where he has been engaged in research on optical fiber design and related measurement techniques. Mr. Shimizu is a member of Japan Society of Applied Physics.

Takashi Matsui was born in Hokkaido, Japan, in 1978. He received B.E., M.E., and Ph.D. degrees in electronic engineering from Hokkaido University, Sapporo, Japan, in 2001, 2003, and 2008, respectively. In 2003, he joined NTT Access Network Service Systems Laboratories, Ibaraki, Japan. He has been engaged in research on optical fiber design technique.

Chisato Fukai was born in Saitama, Japan, in 1976. She received an M.E. degree in functional materials science from Saitama University, Saitama, Japan, in 2001. In 2001, she joined NTT Access Network Service Systems Laboratories, Tsukuba, Ibaraki, Japan, where she has been engaged in research on optical fiber design and related measurement techniques.

Toshio Kurashima was born in Nagano, Japan, in 1961. He received B.E., M.E., and D.E. degrees in electronic engineering from the University of Electro-Communications, Tokyo, Japan, in 1986, 1988, and 1997, respectively. In 1988, he joined NTT Transmission Systems Laboratories where he engaged in research on optical fiber distributed sensing techniques. He is now a Senior Research Engineer, Supervisor of NTT Access Network Service Systems Laboratories. He received the IEICE Excellent Paper Award and Young Engineer Award in 1991 and 1992, and the Outstanding Paper Award of the International Wire and Cable Symposium in 1995.